

Effect of Plasma Composition on the Interpretation of Faraday Rotation

Kiwan Park^{1*} and E.G. Blackman^{1†}

¹*Department of Physics and Astronomy, University of Rochester, Rochester, NY 14627, USA*

ABSTRACT

Faraday rotation (FR) is widely used to infer the orientation and strength of magnetic fields in astrophysical plasmas. Although the absence of electron-positron pairs is a plausible assumption in many astrophysical environments, the magnetospheres of pulsars and black holes and their associated jets may involve a significant pair plasma fraction. This motivates being mindful of the effect of positrons on FR. Here we derive and interpret exact expressions of FR for a neutral plasma of arbitrary composition. We focus on electron-ion-positron plasmas in which charge neutrality is maintained by an arbitrary combination of ions and positrons. Because a pure electron-positron plasma has zero FR, the greater the fraction of positrons the higher the field strength required to account for the same FR. We first obtain general formulae and then specifically consider parameters relevant to active galactic nuclei (AGN) jets to illustrate the significant differences in field strengths that FR measurements from radio frequency measurements. Complementarily, using galaxy cluster core plasmas as examples, we discuss how plasma composition can be constrained if independent measurements of the field strength and number density are available and combined with FR.

Key words: magnetic fields; plasmas; galaxies; jets; radio continuum: general; ISM: magnetic fields; methods: observational

1 INTRODUCTION

Faraday rotation (FR) describes the effect by which the electric field vector of propagating electromagnetic (EM) radiation rotates as it propagates through a magnetized plasma. The EM waves interact with charged particles such that the left and right handed components experience different refractive indices and propagate at different phase velocities. The net electric field vector rotates as the wave propagates. The total amount of this FR between source and observer depends on the strength and orientation of the intervening magnetic field along the line of sight, the plasma density and the plasma composition. FR has been used, for example, to constrain the strength, gradient, and direction of magnetic field in AGN jets (Asada et al. 2002, 2008; Attridge et al. 2005; Zavala & Taylor 2005), galaxy clusters (REF) and the Galactic ISM (REF).

Typically, calculations of FR are made for a neutral ion-electron plasma. While this is a good approximation for the plasma of the Galactic ISM and galaxy clusters, it is less reliable for magnetospheres and outflows around neutron stars and black holes. In particular, constraining the composition of jets in active galactic nuclei (AGN) is obser-

ationally difficult because only the electrons or positrons radiate efficiently so free energy in protons is hard to directly to detect. The plausible predominance of electron-plasma in the magnetosphere of the black hole and the uncertainty as to whether jets emanate directly from its magnetosphere (Blandford & Znajek 1977) or from the surrounding accretion disk (Livio, Ogilvie & Pringle 1999) has contributed to making the composition determination a long standing puzzle. The basic question of how far a jet would be force-free (Li et al. (2006)) is also a fundamental issue. Indirect theoretical constraints on AGN jet plasma composition reach mixed conclusions: Celotti & Fabian (1993) and Ghisellini (2008) favor predominately electron-proton jets, whilst Reynolds et al. (1996) favors a predominantly electron-positron jet for M87. Hubbard & Blackman (2006) argued that on the largest scales, stellar wind mass loading will significantly proton load the jet regardless of its initial composition. It is therefore important to identify possible new techniques for determining jet plasma composition and to be aware of its effect on measurements such as FR.

With the above motivations in mind, we calculate the effect of plasma composition on FR from first principles. In section 2 we first derive the general exact formula for FR in an arbitrary neutral plasmas. We then consider the special cases of a pure ion electron plasmas and an ion-electron-positron plasma. In section 3 we solve the exact and high

* E-mail: pkiwan@pas.rochester.edu

† E-mail: blackman@pas.rochester.edu

frequency approximations to the general FR equation and show quantitatively how plasma composition leads to degeneracies in the electron number density n_e , the magnetic field B . We discuss how these degeneracies can in principle be used to constrain the plasma composition in AGN jets, and conclude in section 4.

2 GENERALIZED FARADAY ROTATION

2.1 Formalism for Arbitrary Neutral Plasmas

To formally derive FR for an arbitrary neutral plasma, we assume a cold neutral plasma in a background external magnetic field \vec{B}_{ex} , subject to a perturbation from a propagating electromagnetic wave. (The cold plasma approximation for FR has been shown to be effective for the electron contribution to FR even for quasi-relativistic plasmas (Skilling 1971), and we discuss this further below Eq.(16)). For the electric field \vec{E} , magnetic field \vec{B} and induced particle velocity \vec{v}_s (where the index s indicates particle species) we write

$$\begin{aligned}\vec{E} &= \vec{E}_1, \\ \vec{B} &= \vec{B}_1 + \vec{B}_{ex}, \\ \vec{v}_s &= \vec{v}_{s1},\end{aligned}\quad (1)$$

where \vec{E}_1 and \vec{B}_1 are perturbations such that $|B_1/B_{ex}| \ll 1$, $|E_1/B_{ex}| \ll 1$ and $v_{s1} \ll c$. We also assume a neutral plasma so that

$$\sum_s n_{s0} e_s = 0, \quad (2)$$

where n_{s0} is the unperturbed density of a particle of species s , and e_s is charge of particle of species s .

Using the above formalism, Maxwell equations become (e.g. Gurnett & Bhattacharjee (2005)):

$$\nabla \times \vec{E}_1 = -\frac{1}{c} \frac{\partial \vec{B}_1}{\partial t}, \quad \nabla \times \vec{B}_1 = \frac{4\pi}{c} \vec{J} + \frac{1}{c} \frac{\partial \vec{E}_1}{\partial t}. \quad (3)$$

If the current density $\vec{J} \equiv \sum_s n_{s0} e_s \vec{v}_{s1} = 0$, then E_1 & B_1 are decoupled, resulting in the plane wave vacuum equations. However a finite \vec{J} and the Lorentz force equation

$$m_s \frac{d\vec{v}_s}{dt} = e_s (\vec{E}_1 + \frac{1}{c} \vec{v}_s \times \vec{B}_{ex}) \quad (4)$$

imply that in general, that \vec{E} , \vec{B} , and \vec{v}_s are all coupled.

To quantify the interaction between the particles and EM fields, we take $\vec{v}_s, \vec{E}_1 \propto e^{i(\vec{k} \cdot \vec{x} - \omega t)}$ so Eq.(4) becomes

$$\vec{v}_s = \frac{ie_s}{m_s \omega} (\vec{E}_1 + \frac{\vec{v}_s}{c} \times \vec{B}_{ex}) = \frac{ie_s}{m_s \omega} (\vec{E}_1 + \frac{\vec{v}_s}{c} \times \frac{m_s c \vec{\omega}_{cs}}{e_s}), \quad (5)$$

where $\omega_{cs} = e_s B_{ex} / m_s c$ is the cyclotron frequency of species s . The current density can then be expressed as the product of a conductivity tensor and the \vec{E}_1 field, namely $\vec{J} = \overleftrightarrow{\sigma} \cdot \vec{E}_1$, where the conductivity tensor is given by (Ashok 2004)

$$\sigma_{ij} = \sum_s \frac{i n_{s0} e_s^2}{m_s \omega [1 - (\frac{\omega_{cs}}{\omega})^2]} \left(\delta_{ij} - \frac{\omega_{cs} i \omega_{cs, j}}{\omega^2} - \frac{i}{\omega} \epsilon_{ijk} \omega_{cs, k} \right).$$

We now take $\vec{B}_{ex} = (0, 0, B)$ so that the components of Eq.(5) become

$$-i\omega m_s v_{sx} = e_s (E_{1x} + \frac{v_{sy}}{c} B),$$

$$\begin{aligned}-i\omega m_s v_{sy} &= e_s (E_{1y} - \frac{v_{sx}}{c} B), \\ -i\omega m_s v_{sz} &= e_s E_{1z},\end{aligned}\quad (7)$$

and, the conductivity tensor becomes

$$\overleftrightarrow{\sigma} = \sum_s \frac{n_{s0} e_s^2}{m_s} \begin{pmatrix} \frac{-i\omega}{\omega_{cs}^2 - \omega^2} & \frac{\omega_{cs}}{\omega_{cs}^2 - \omega^2} & 0 \\ \frac{\omega_{cs}}{\omega_{cs}^2 - \omega^2} & \frac{-i\omega}{\omega_{cs}^2 - \omega^2} & 0 \\ 0 & 0 & \frac{i}{\omega} \end{pmatrix}. \quad (8)$$

Eq.(3) with $\vec{\nabla} \rightarrow i\vec{k}$ then becomes

$$\vec{k} \times (\vec{k} \times \vec{E}_1) + \frac{\omega^2}{c^2} (1 - \frac{4\pi}{i\omega} \overleftrightarrow{\sigma}) \cdot \vec{E}_1 = 0. \quad (9)$$

from which the secular equation for the FR effect is

$$\begin{pmatrix} S - n^2 & -iD & 0 \\ iD & S - n^2 & 0 \\ 0 & 0 & P \end{pmatrix} \begin{pmatrix} E_{1x} \\ E_{1y} \\ E_{1z} \end{pmatrix} = 0, \quad (10)$$

where $S \equiv 1 - \sum_s \frac{\omega_{ps}^2}{\omega^2 - \omega_{cs}^2}$, $D \equiv \sum_s \frac{\omega_{cs} \omega_{ps}^2}{\omega(\omega^2 - \omega_{cs}^2)}$, $P \equiv 1 - \sum_s \frac{\omega_{ps}^2}{\omega^2}$ and the plasma frequency and wave vector are given respectively by $\omega_{ps}^2 = \frac{4\pi n_s e_s^2}{m_s}$ and $\vec{k} = \frac{n\omega}{c} \hat{z}$.

The solution of Eq.(10) for refractive index n produces non-trivial FR when the two solutions for n are distinct, corresponding to left and right handed polarizations; $n_L^2 = S - D$, $n_R^2 = S + D$ with two associated \vec{E}_1 field eigenvectors. The transverse (x, y) components of \vec{E}_1 for each refractive index are of the same magnitude but have different phases, that is, $E_L = (E_0, -iE_0, 0)$, $E_R = (E_0, iE_0, 0)$, where $\pm i$ arises from the differentiation of velocity and position over time in the Lorentz force law. The equal amplitude of the transverse E field components then imply circularly polarized waves.

The different phase velocities ($c/n_L, c/n_R$) cause the propagating left and right handed circularly polarized waves to experience a net phase angle difference when they propagate over the same distance. As a result, the net electric field phase angle ($\phi = \text{Tan}^{-1}(E_y/E_x)$) that comes from the superposition of these handed waves rotates along the propagating distance. This is the FR. The change ϕ along the propagation distance is

$$\begin{aligned}\frac{d\phi}{dz} &= \frac{1}{2} (k_L - k_R) \\ &= \frac{\omega}{2c} \left(\sqrt{1 - \sum_s \frac{\omega_{ps}^2}{\omega(\omega - \omega_{cs})}} - \sqrt{1 - \sum_s \frac{\omega_{ps}^2}{\omega(\omega + \omega_{cs})}} \right).\end{aligned}\quad (11)$$

Having derived the general formalism for a neutral plasma of arbitrary composition and the exact equation for FR (Eq.(11)), we note that Hall & Shukla (2005) considered FR in an ion-electron positron plasma producing the approximate analytical result

$$\frac{d\phi}{dz} \sim Z_i n_i \frac{2\pi e^3 B}{m_e^2 c^2 \omega^2}, \quad (12)$$

(6) where Z_i is the ion charge number. Eq.(12) agrees with Eq.(11) in the high frequency limit for an ion-electron-positron plasma, a point we will return to in section 2.3. Eq.(12) indicates there is no FR in case of an electron-positron pair plasma ($n_i = 0$). For $n_i \neq 0$, ions generate the FR by breaking the symmetry of a pair plasma.

2.2 Ion-electron plasma

For a pure (hydrogen) ion-electron plasma, Eq.(2) takes the form $n_e + n_i = 0$, where n_e and n_i are the electron and hydrogen ion number densities. The summation over s in Eq.(11) also involves terms corresponding to electrons and ions respectively. However, because of the large ion to electron mass ratio $m_i/m_e = 1836$, the ion terms are typically ignored (e.g. Asada et al. (2002, 2008); Zavala & Taylor (2005)). Then the rotated angle integrated along the line of sight for the distance l (e.g. Reynolds et al. (1996)) becomes

$$\begin{aligned} \phi &\simeq \int_0^l \frac{\omega}{2c} \left(\sqrt{1 - \frac{\omega_{pe}^2}{\omega(\omega - \omega_{ce})}} - \sqrt{1 - \frac{\omega_{pe}^2}{\omega(\omega + \omega_{ce})}} \right) \cdot dz \\ &\sim \frac{2\pi e^3}{m_e^2 c^2 \omega^2} \int_0^l n_e B \cos \theta dz \\ &= \left(\frac{e^3}{2\pi m_e^2 c^4} \int_0^l n_e B \cos \theta dz \right) \cdot \lambda^2 \equiv RM \cdot \lambda^2, \end{aligned} \quad (13)$$

where the second relation follows for $\omega \gg \omega_{pe}, \omega_{ce}$. The general procedure for determining RM is to measure ϕ at multiple wavelengths and infer a slope of the ϕ vs. λ line.

2.3 Ion-electron-positron plasma

For the hydrogen ion-electron-positron case Eq.(2) becomes

$$-en_e + en_{e^+} + en_i = 0, \quad (14)$$

where n_{e^+} is the positron number density. We now define $X \equiv n_{e^+}/n_e$ so that

$$n_{e^+} = n_e X, \quad n_i = n_e(1 - n_{e^+}/n_e) = n_e(1 - X). \quad (15)$$

Eq.(11) then becomes

$$\begin{aligned} \frac{d\phi}{dz} &= \frac{\omega}{2c} \left(\sqrt{1 - \frac{\omega_{pe}^2}{\omega(\omega - \omega_{ce})} - \frac{\omega_{pe^+}^2}{\omega(\omega - \omega_{ce^+})} - \frac{\omega_{pi}^2}{\omega(\omega - \omega_{ci})}} \right. \\ &\quad \left. - \sqrt{1 - \frac{\omega_{pe}^2}{\omega(\omega + \omega_{ce})} - \frac{\omega_{pe^+}^2}{\omega(\omega + \omega_{ce^+})} - \frac{\omega_{pi}^2}{\omega(\omega + \omega_{ci})}} \right) \\ &= \frac{\omega}{2c} \left(\sqrt{1 - \frac{4\pi e^2 n_e}{m_e} \left(\frac{1}{\omega + \frac{eB}{m_e c}} + \frac{X}{\omega - \frac{eB}{m_e c}} + \frac{1-X}{1836\omega - \frac{eB}{m_e c}} \right)} \right. \\ &\quad \left. - \sqrt{1 - \frac{4\pi e^2 n_e}{m_e} \left(\frac{1}{\omega - \frac{eB}{m_e c}} + \frac{X}{\omega + \frac{eB}{m_e c}} + \frac{1-X}{1836\omega + \frac{eB}{m_e c}} \right)} \right) \\ &= \frac{\omega}{2c} \left(\sqrt{1 - q_L} - \sqrt{1 - q_R} \right), \end{aligned} \quad (16)$$

where q_L represents the second term under the first square root of the second equality and q_R represents the second term under the second square root of the second equality.

Eq.(11), (12) and (16) presume a cold plasma and it is instructive to comment on the validity of these expressions for a warm plasma. For the latter, motions of charged particles are influenced by thermal effects in addition to the electromagnetic force and to express the current density the solution of Vlasov equation is necessary (e.g. Gurnett & Bhattacharjee (2005), chapt. 9). Skilling (1971) studied FR for a warm ion-electron plasma and found that for large frequencies away from resonances, the correction to the electron contribution to FR is small compared to the cold

plasma term. However, for a pair plasma in which the electron and positron cold plasma terms cancel exactly, warm plasma correction terms would not cancel exactly and a finite contribution would remain as the positron and electron correction terms do not cancel. We ignore these small corrections for present purposes and leave further discussion for future work.

In the high frequency limit, $q_L \ll 1$ and $q_R \ll 1$, and we can approximate Eq.(16) as

$$\begin{aligned} \frac{d\phi}{dz} &\simeq \frac{2\pi e^3}{m_e^2 c^2} n_e B (1 - X) \left(\frac{1}{\omega^2 - (\frac{eB}{m_e c})^2} - \frac{1}{1836^2 \omega^2 - (\frac{eB}{m_e c})^2} \right) \\ &\sim \frac{2\pi e^3}{m_e^2 c^2} n_e B (1 - X) \left(\frac{1}{\omega^2} - \frac{1}{1836^2 \omega^2} \right). \end{aligned} \quad (17)$$

Using Eq.(15), then Eq.(17) is the same as Eq.(12).

For a pure neutral pair plasma ($X=1$), the right side of Eq.(16) (or (17)) vanishes. The FR vanishes because the equal mass of positrons and electrons induce the same phase speeds for oppositely handed EM waves. This contrasts the limit of the previous subsection of a pure neutral (hydrogen) ion-electron plasma ($X=0$), for which the mass asymmetry leads to unequal phase speeds of the oppositely handed waves and a finite right side of Eq.(16). In general, for $0 \leq X \leq 1$ with n_e , B_{ex} and source distance fixed, the right side of Eq.(16) decreases with increasing X . We discuss solutions of Eq.(16) in the next section.

Note that the exact FR expression (16) has singularities when the wave frequency of the EM wave coincides with the particle cyclotron frequencies, i.e. at $\omega = eB/m_e c = 1.76 \times 10^7 B$ (for electrons and positrons) and $eB/m_i c = 9571 B$ (for ions). The FR would exhibit sharp resonance features near the singular points, allowing the B field to be inferred in principle. However, for applications to extended jets of AGN and larger scale systems, these resonant frequencies are generally small compared to the relevant \sim GHz frequencies.

3 ASTROPHYSICAL IMPLICATIONS

3.1 General Implications of Plasma Composition

Figs.1 and 2 show solutions to the exact expression Eq.(16) and the approximation Eq.(17) for n_e , B and X at fixed values of RMs (2592 rad/m² in Fig.1. and 1000 rad/m² in Fig.2). The RMs were converted into rotation angles for cm scale at $\lambda = 1.35$ cm (22.2GHz). The FR in Fig.1 corresponds to 3.63 pc (749 Mpc \times 0.5 mas, C1 region) from the core of AGN jet 3C 273 from Zavala & Taylor (2001). From synchrotron emission, Savolainen et al. (2006) calculated the total magnetic field to be ($B \sim 0.06$ G) in this region. If this were the line of sight field, Fig.1(b) shows that $n_e \geq 0.05$ cm⁻³ for RM (2592 rad m⁻²), the minimum n_e occurring at $X = 0$. Fig.2(c) shows a complementary example for values appropriate for a typical X-ray cluster (Jaffe (1980)) with $n_e \sim 0.003$ cm⁻³ and RM ~ 1000 rad m⁻². The standard assumption that $X = 0$ for a known distance leads directly to the inference that $B \sim 1\mu$ G (Jaffe 1980). But for any $X < 1$, Fig.2(b) for example, shows how much stronger the field could be.

For fixed values of RM, Figs.1(a), and 2(a) show that n_e and B behave oppositely for each value of X : As n_e increases (decreases), B decreases (increases). These trends

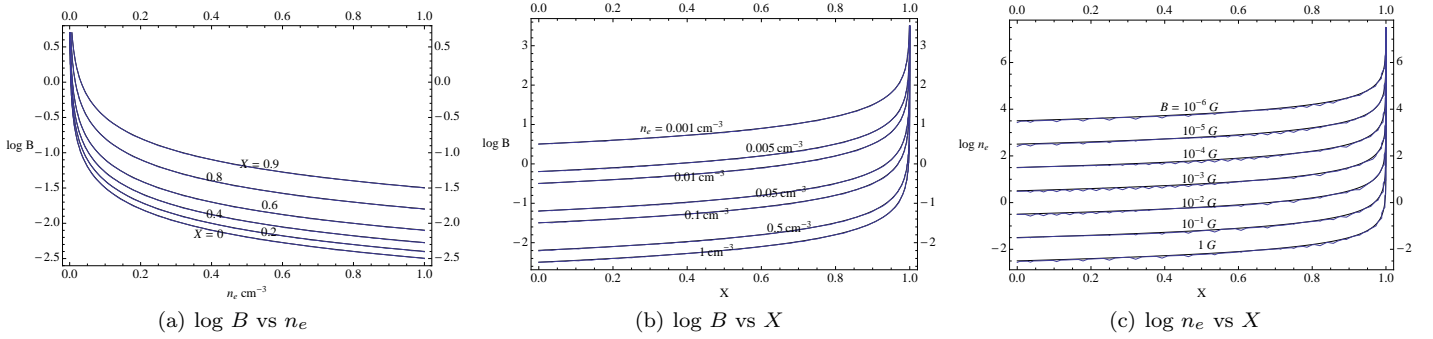


Figure 1. Plots of n_e , B and X . All panels use a fixed $RM = 2592 \text{ rad } m^{-2}$ in Zavala & Taylor (2001) (Fig.3). The line of sight B field is estimated at $\sim 0.5 \text{ mas}$ ($\sim 3.63 \text{ pc}$) from the core. All of the plots were made using both Eq.(16) and Eq.(17) with $\lambda = 1.35 \text{ cm}$ (22.2 GHz). The plots of each equation were overlapped highlighting the efficacy of the approximate equation. The original observation frequency is 8GHz but any frequency gives the same RM.

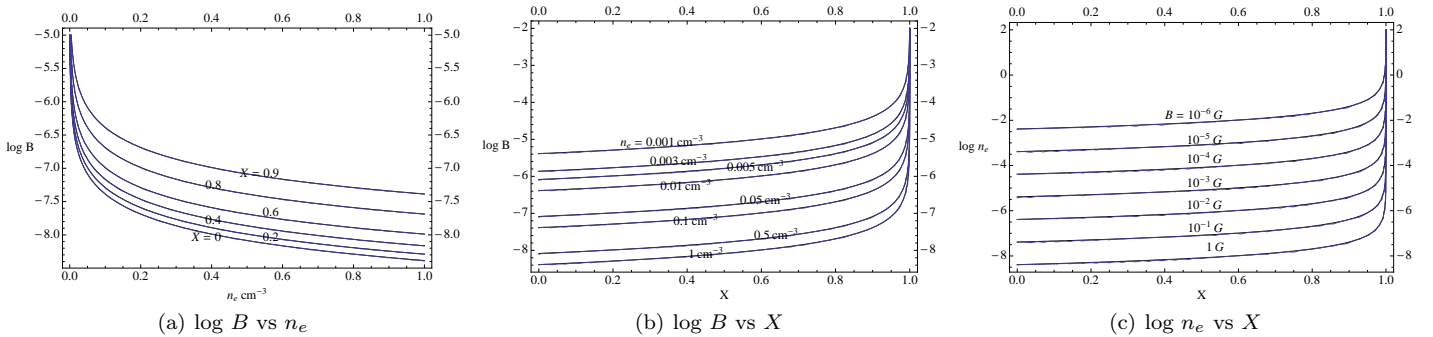


Figure 2. Same as Fig.1. but using $RM \sim 1000 \text{ rad } m^{-2}$, path length $l = 300 \text{ kpc}$, in an X-ray cluster core Jaffe (1980) with $\lambda = 1.35 \text{ cm}$ (22.2 GHz) Again both Eq.(16) and Eq.(17) were used for the plots.

reflect that the RM is roughly proportional to the field and the density. Figs.1(a), 1(b), 2(a), and 2(b) show that as X increases (decreases), B and n_e increase (decrease) respectively. These trends result because an increasing X means a higher fraction of pair plasma. The latter contributes zero FR so that a higher B or n_e is needed for a fixed RM. Figs.1(c), and 2(c) reflect these same trends.

In all panels, the lines resulting from Eq.(16) are indistinguishable from those obtained using Eq.(17) for the parameters used, highlighting the efficacy of the latter. Figs.2(a), 2(b) and 2(c) are very similar to Figs.1(a), 1(b) and 1(c) as only the vertical axis scales are different due to the different RM choices. Overall, the figures show how an unknown plasma composition X implies degeneracies in the values n_e and B , or complementarily, how independent measures of n_e and B can be combined with an RM to constrain X .

3.2 Further Discussion of Applications

If the RM and two of the three quantities n_e , X and B are independently known, the FR equation is exactly determined. However, even if only one variable and RM are known, the other variables can be constrained.

There have been efforts to interpret the RM with a subset of independently measured variables n_e , B and T . For example, Zavala & Taylor (2002) calculated the B field in M87 using the RM and an independently determined n_e .

For $RM = -4000 \text{ rad } m^{-2}$, Eq.(13) was used to get $B \sim 15 \mu\text{G}$, but $X = 0$ was assumed. We can revisit the interpretation of the measured RM without assuming $X = 0$ a priori. As seen in Fig.3(a), the cross point of $B \sim 15 \mu\text{G}$ and $RM = -4000 \text{ rad } m^{-2}$ with $n_e = 1100 \text{ cm}^{-3}$ (dashed line) is $X = 0$. In contrast, if we suppose that $B = 200 \mu\text{G}$, which corresponds to the thermal equipartition condition when $T \sim 10^4 \text{ K}$ ($n_e k_B T = B^2 / 8\pi$ where B is the mean line of sight field that causes FR, e.g. Gabuzda et al. (2008)), different X values result: For $RM = 9000 \text{ rad } m^{-2}$ and $-4000 \text{ rad } m^{-2}$, the X values are 0.83 and 0.92 respectively. The corresponding n_e values are 913 and 1012 cm^{-3} . If instead magnetic pressure dominates (e.g. dominant ($\beta \equiv P_g / P_B = 8\pi n_e k_B T / B^2 < 1$)), then X increases as shown in Fig.3.

As another set of examples showing the degeneracy between B and X , we consider the independently measured RM, n_e , B and T for clusters A400, A1795 and A2199 (Eilek & Owen 2002) which respectively include radio sources 3C75, 4C46.42 and 3C338 to obtain Fig.3(b). B is also the mean line of sight field but we note that the definition of the magnetic pressure ($P_B = 3 < B_{\parallel} >^2 / 8\pi$) is different from that of Zavala & Taylor (2002). We have taken this into account when interpreting their respective data. There, instead of assuming $X = 0$, as is normally done to obtain the B , we chose selected field strengths (straight lines on the plot) and identify the constraints this places on X by where these lines intersect with the curves. For ex-

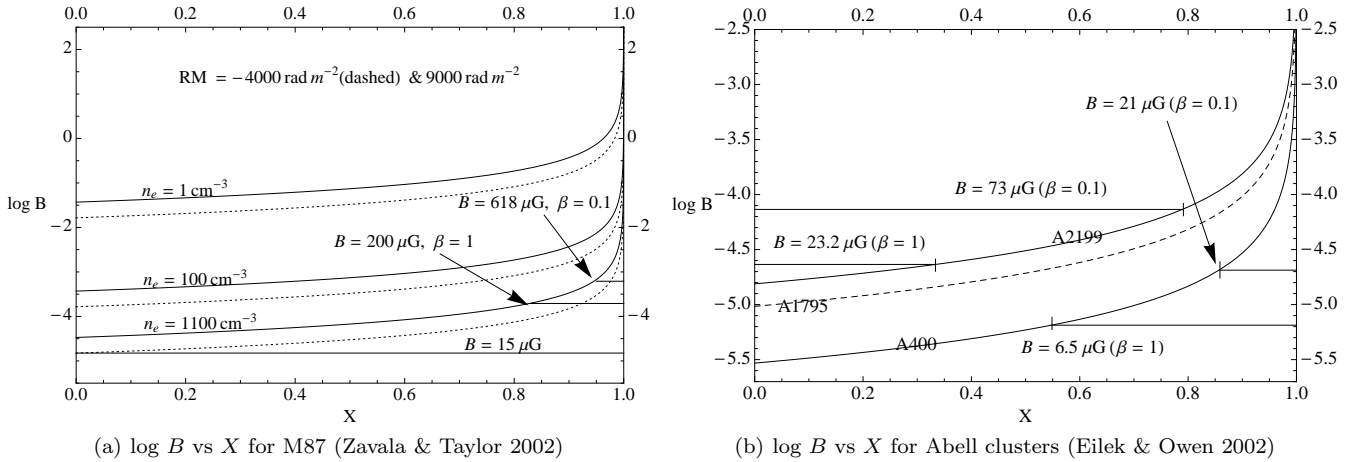


Figure 3. These $\text{Log}B$ vs X plots were made using RM , B , n_e and T from Zavala & Taylor (2002) and Eilek & Owen (2002). The rotation angle for (a) was converted from the $\text{RM} = -4000 \text{ rad m}^{-2}$ (dashed line) and 9000 rad m^{-2} (solid line) at $\lambda = 1.35 \text{ cm}$ (22.2 GHz). For (b), each data point for RM (50, 1500, 750 rad m^2); n_e (0.0021, 0.064, 0.02 cm^{-3}); and T (1.5, 5.1, 1.2 keV) where the values in parentheses are for A400, A1795, A2199 respectively, were also plotted for 22.2GHz. The values of β correspond to the particular cluster which the separate lines of B intersect, explaining why different values of the field correspond to the same $\beta = 0.1$ for A400 and A2199.

ample, for A400, if magnetic and thermal pressures were in equipartition ($\beta = 1$), the data would imply $X = 0.55$ (Here $n_e = 0.0021 \text{ cm}^{-3}$, $n_{e+} = 1.155 \times 10^{-3} \text{ cm}^{-3}$, $n_i = 9.45 \times 10^{-4} \text{ cm}^{-3}$). However, if magnetic pressure were dominant (e.g. $\beta = 0.1$), then $X = 0.86$ ($n_e = 0.0021 \text{ cm}^{-3}$, $n_{e+} = 1.806 \times 10^{-3} \text{ cm}^{-3}$, $n_i = 2.94 \times 10^{-4} \text{ cm}^{-3}$). The extent to which X differs from zero in clusters could depend on how close to a radio source core the RM is measured as one would indeed expect $X = 0$ far away from radio jets. As better spatial coverage of both FR and synchrotron constraints become available for jets, the use of plots such as those of Fig.1 and 2 become more powerful.

4 CONCLUSIONS

Assuming plasma neutrality, we have generalized the calculation of FR for a neutral plasma containing electrons, positrons, and ions. Positrons contribute equally and oppositely to electrons under the approximations considered. Thus as the ratio of positrons to electrons X increases from 0 to 1, the FR weakens for a given line of sight magnetic field and density. Correspondingly, for a given RM , a larger value of X would imply a field strength and or electron density in excess of that inferred for $X = 0$.

While $X = 0$ is often assumed for astrophysical plasmas, this assumption is not necessarily valid for jets and magnetospheres of black holes and neutron stars, where in fact it is of interest to independently determine X . We have shown quantitatively the degeneracies in the space of parameters n_e , X , and B and how they can be constrained. In principle, if independent data on B and n_e can be obtained, then a given RM measurement can be used to obtain X . The pursuit of X has been particularly elusive in the context of AGN jets and we hope that the calculations herein provide a tool toward this goal, and help motivate the pursuit of further data.

ACKNOWLEDGMENTS

KP acknowledges a Horton Graduate Fellowship from the Laboratory for Laser Energetics at the Univ. of Rochester. EGB acknowledges support from NSF grants AST-0406799, AST-0807363, and NASA grant ATP04-0000-0016.

REFERENCES

- Asada K., Inoue M., Uchida Y., Kameno S., Fujisawa K., Iguchi S., Mutoh M., 2002, PASJ, 54, L39
- Asada K., Inoue M., Kameno S., Nagai H., 2008, ApJ, 675, 79
- Ashok D., 2004, Lectures on Electromagnetism, 1st edn., 389p, Rinton Press
- Attridge J. M., Wardle J. F. C., Homan D. C. 2005, ApJ, 633, L85
- Begelman M. C., Blandford R. D., Rees M. J., 1984, Rev. Mod. Phys., 56, 255
- Blandford R. D., Znajek R. L., 1977, MNRAS, 179, 433
- Celotti A., Fabian A.C., 1993, MNRAS, 264, 228
- Li H., Lapenta G., Finn J. M., Li S., Colgate S. A., 2006, ApJ, 643, 92
- Eilek Jean A., Owen Frazer N., 2002, ApJ, 567, 202
- Gabuzda D. C., Pushkarev A. B., Garnich N. N., 2001, MNRAS, 327, 1
- Gurnett D. A., Bhattacharjee A., 2005, Introduction to Plasma Physics, 94p, Cambridge University Press
- Ghisellini G., 2008, IJMPD, 17, 1491
- Hall J.O., Shukla P.K., 2005, Phys. Plasma, 12, 084507
- Hubbard, A., & Blackman, E.G., 2006, MNRAS, 371, 1717
- Jaffe W., 1980, ApJ. 241, 925
- Kulsrud R. M., 2005, Plasma Physics for Astrophysics, 262p, Princeton University Press
- Kronberg P. P., Perry J. J., Zukowski E. L. H., 1990, ApJ, 355, L31
- Livio M., Ogilvie G. I., Pringle J. E., 1999, ApJ, 512, 100
- Michel F. C., 1982, Rev. Mod. Phys., 54, 1 Manch-

6 *Kiwan Park and E.G. Blackman*

- ester R. N., Taylor J. H., 1978, Pulsars, 1st edn., 134p,
W.H.Freeman & Co Ltd
- Reynolds, C.S., Fabian, A.C., Celotti, A., Rees, M.J. 1996b,
MNRAS, 283, 873
- Savolainen T., Wiik K., Valtaoja E., Tornikoski M., 2006,
ASP, 446, 71-85
- Skilling J., 1971, PhFl, 14, 2523
- Zavala R. T., Taylor G. B., 2005, ApJ, 626, L73
- Zavala R. T., Taylor G. B., 2001, ApJ, 550, L147
- Zavala R. T., Taylor G. B., 2002, ApJ, 566, L9-L12